Nanorod Cuprous Oxide as Anode for Sodium Ion Battery

Jiahui Zhou, Wei Sun, Yue Yang**

School of Minerals Processing and Bioengineering, Central South University, Changsha 410083, China
*E-mail: sunmenghu@csu.edu.cn, eric1911@126.com

Given the better electrical conductivity and electrochemical performance of one-dimensional materials compared with multi-dimensional materials, high-purity one-dimensional nano-sized cuprous oxide rods, as anode materials for sodium ion batteries, were synthesized via a facile hydrothermal method. A rod width of approximately 150 nm and X-ray diffraction patterns were confirmed by scanning electron microscopy and X-ray diffraction. Compared with irregular nano-sized cuprous oxide, cuprous oxide nanorods demonstrated a high initial capacity of 380 mAh·g^{-1} and good reversible capacity of 245 mAh·g^{-1} at a capacity retention of 59% after 50 cycles. These results demonstrated the great application potential of the proposed material for sodium ion batteries. In addition, the Na ion diffusion coefficient have been quantitative analyzed by EIS, reflecting the good diffusion coefficient in one-dimensional materials. This work might provide a reference for the selection of the shape of energy storage materials.

1. INTRODUCTION

Sodium ion batteries have attracted great attention as a potential substitute for lithium ion batteries and have become a research hotspot in the field of energy storage materials, given that sodium resources are extremely abundant and have similar chemistry to lithium.[1] However, the ionic radii of sodium ions are larger compared with those of lithium ions. Hence, the anode materials that are widely used for lithium ion battery, such as graphite, cannot be applied for sodium ion batteries.[2] Therefore, developing new materials with excellent sodium storage performance has become one of the toughest challenges in the field of sodium ion batteries. Up to now, a large number of anode materials for sodium ion batteries, such as carbon-based materials, metal oxides, and metal sulfides, have been extensively prepared. Among these potential anode materials, copper-based oxides have attracted great attention due to their chemical stability, non-toxicity, and abundance from earth resources.[3]

At present, various morphologies of copper oxide nanomaterials, such as nanoparticles[4], nanospheres[5], and nanocubes[6], are mainly synthesized by hydrothermal, solvothermal, sonochemical, and microwave and template methods. These different forms of cuprous oxides synthesized by these predecessors have significant challenges caused by poor electrochemical cycle performance and low electrical conductivity.[7] Compared with the above shapes, one-dimensional materials, such as rods, have short lithium ion diffusion channels and small volume expansion, resulting in enhanced conductivity and cycle performance.[8] In this study, one-dimensional rod-shaped cuprous oxide with good morphology was synthesized via a facile hydrothermal method. Meanwhile, cyclic performance and AC impedance tests were conducted to investigate the electrochemical performance of cuprous oxide.
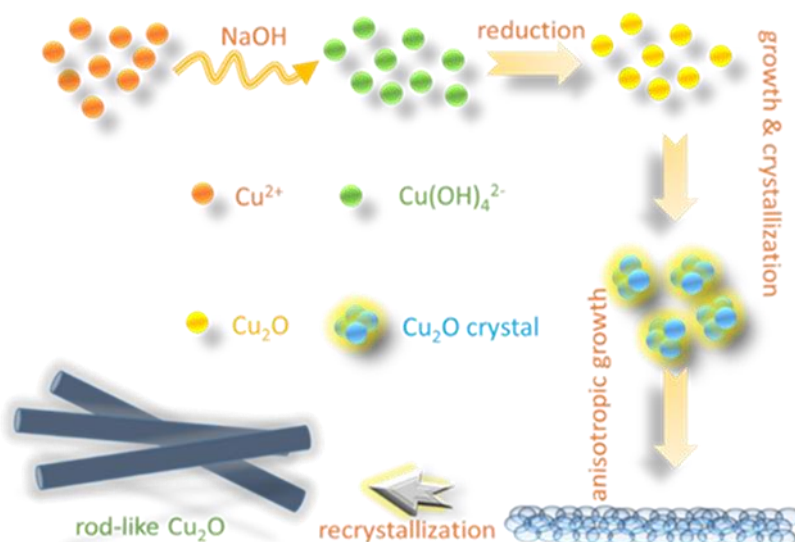
2. EXPERIMENTAL SECTION

2.1 Materials

The reagents used, namely, copper sulfate pentahydrate, sodium hydroxide, cetyltrimethylammonium bromide, glucose, chloride dehydrate, and sodium borohydride, are of analytical grade and purchased from Sinopharm Chemical Reagent Co., Ltd.

2.2 Material preparation

Cu_2O nanorod: First, 50 ml of 160 mmol/l $Cu(OH)_4^{2-}$ solution was prepared by adding 50 ml of 60 mol·l^{-1} NaOH solution into 8 mmol copper sulfate pentahydrate. Second, 6 mmol cetyltrimethylammonium bromide was added to the $Cu(OH)_4^{2-}$ solution and stirred vigorously for 0.5 h at 70 °C with a magnetic stirrer to completely dissolve cetyltrimethylammonium bromide.

Scheme 1. Schematic of the formation process of Cu_2O rod

Third, 0.8 mmol of glucose was added to the above solution to obtain a homogeneous mixture, which was then allowed to stand at 25 °C for 1 h. Fourth, the above mixture was charged into a 100 ml autoclave and reacted at 120 °C for 12 h. Finally, after the reaction, the final product was removed and washed three times with absolute ethanol and distilled water, centrifuged at 10,000 rpm, and dried at 25 °C for 24 h in a vacuum oven. The possible formation process of the cuprous oxide nanorods is shown in Scheme 1.

Cu_2O nanoparticle: 15 mmol chloride dihydrate and 12 ml sodium borohydride were mixed, reacted under stirring for 3 h, centrifuged at 10,000 rpm, washed with distilled water, and dried at 30 °C under vacuum.

2.4 Measurement

The electrochemical performance of the prepared materials was tested by assembling sodium ion batteries with synthetic cuprous oxide nanorods (R-Cu_2O) and cuprous oxide nanoparticles (P-Cu_2O) as anode electrode materials and sodium metal as negative electrode. The anode consists of synthetic cuprous oxide, acetylene black, sodium carboxymethylcellulose in a ratio of 8:1:1. When the anode was prepared using CMC as a binder, the above materials were mixed with deionized water as a solvent, and they were uniformly mixed under magnetic stirring. The obtained slurry was coated on a copper foil, dried in a vacuum oven at 60 ° C for 8 hours, and then used as a final working electrode. The mass loading of anode active material was approximately 0.7–1.0 mg. The assembling sodium ion batteries in a glove box filled with pure Ar atmosphere (H_2O and O_2 levels < 0.1 ppm). Propylene carbonate, 1 mol $NaClO_4$, 5% fluoroethylene carbonate as electrolyte, and Celgard 2400 as separator. Galvanostatic charge–discharge measurements were conducted on a Land-CT2001A instrument at 25 °C in the voltage range of 3.0–0.01 V (vs. Na/Na^+). Electrochemical impedance spectroscopy (EIS) was performed on an electrochemical workstation (Multi Autolab M204) at a frequency range of 10^5–0.01 Hz.

3. RESULT AND DISCUSSION

Scanning electron microscopy was performed to observe the surface morphology of the Cu_2O sample. Figures 1a and 1b show the SEM images of R-Cu_2O and P-Cu_2O, respectively. Figure 1a shows that the morphology of the final product obtained via hydrothermal method is nanorod-shaped. These synthetic rod-shaped cuprous oxides are uniform in size with approximately 150 nm in diameter and have good dispersion, indicating that the synthesis method is very effective. This finding provides new methods and ideas for synthesis of other nanorod materials. Figure 1b shows that P-Cu_2O is nanoparticulate and has a size of approximately 100 nm. The crystal structures of the synthesized cuprous oxide nanorods and cuprous oxide nanoparticle were tested by X-ray diffraction. As seen in Figure 1c, the formation of phase-pure Cu_2O with Pn-3m space group was determined by comparing the obtained XRD patterns with standard JCPDS data. The peaks of the synthesized cuprous oxide nanorods and cuprous oxide nanoparticles can correspond well with the peaks of standard cuprous oxide (JCPDS

No. 78-2076), indicating their highly crystalline nature. This finding is consistent with the standard Cu_2O diffraction peaks, confirming that the products are pure. Since cuprous ions are very susceptible to oxidation in the prepared process of cuprous oxide nanorods, the XPS is used to detect the valence of copper. As shown in Figure 1d, the shake-up satellites doesn't exist at the high-binding energy side of the Cu-2p3/2 (932.6eV), indicating copper has a complete $3d^{10}$ configuration.[9] Thus, this result displays that Cu is +1.

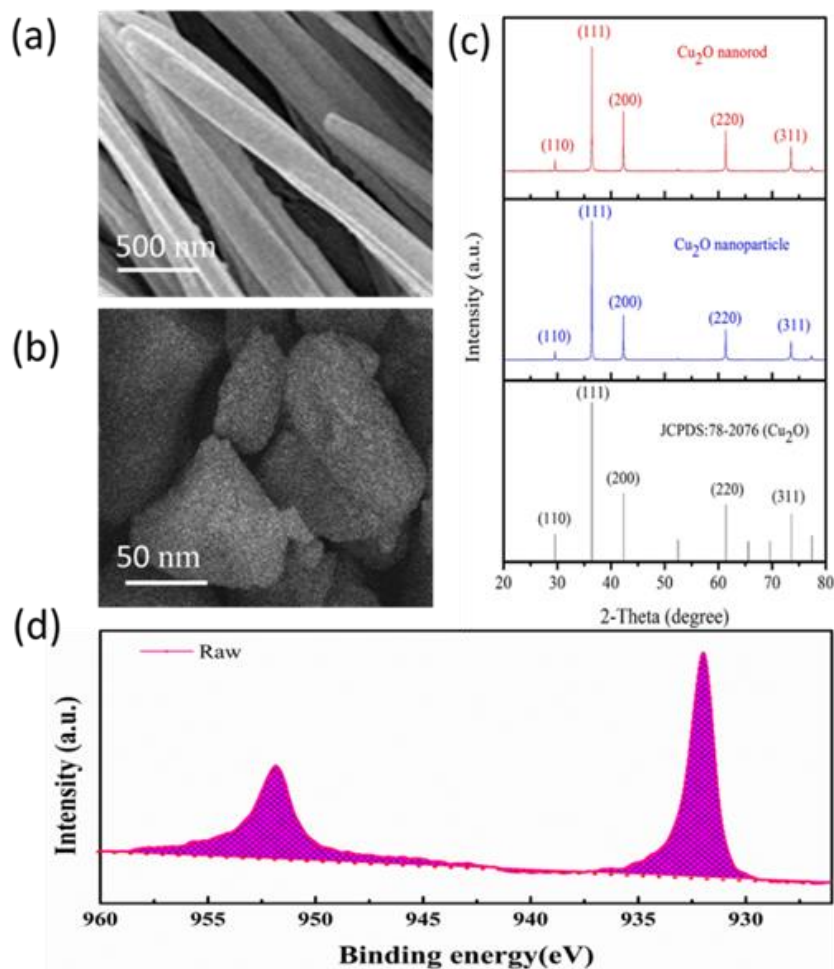**Figure 1.** SEM images of (a) Cu_2O nanorod, (b) Cu_2O nanoparticle. (c) XRD patterns of Cu_2O nanorod and Cu_2O nanoparticle, (d) the high-resolution XPS spectra of Cu.

Charge–discharge measurements and EIS tests were performed to investigate the electrochemical and conductive properties of cuprous oxide nanorods and nanoparticles. Figure 2a shows the electrochemical performance of R-Cu_2O and P-Cu_2O in the first cycle at current density of 100 mA·g^{-1}, the similar charge/discharge platforms have been observed, indicating the similar redox reactions. In addition, P-Cu_2O displays the higher initial capacity than R-Cu_2O, with discharge capacity of 601.5 mAh·g^{-1}. Figure 2b shows the cycle performance and corresponding Coulombic efficiency of a rod-shaped cuprous oxide (R-Cu_2O) electrode and nanoparticulate cuprous oxide (P-Cu_2O) at a current density of 100 mA·g^{-1}.
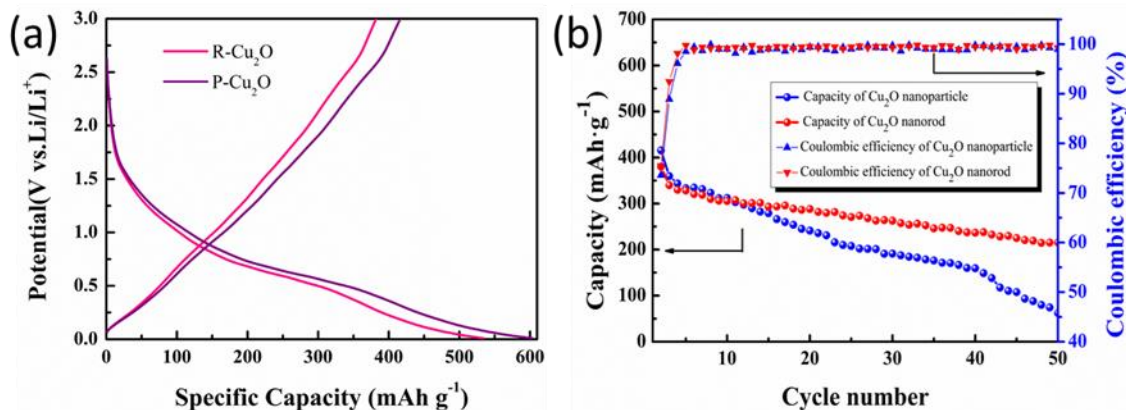
Figure 2. (a) Charge and discharge curve (b) Coulombic efficiency and cycling performance of Cu_2O nanorod and Cu_2O nanoparticle for 50 cycles at 100 $mA \cdot g^{-1}$

Table 1. Comparison of our work versus other previously related studies.

anode material	Preparation method	Morphology	Reversible capacity ($mAh \cdot g^{-1}$)	Current density ($mA \cdot g^{-1}$)	Cycles	Ref.
Cu_2O	chemical precipitation method	spherical	82	100	50	[10]
Cu_2O dense film	electrochemical deposition	film	258	37	50	[11]
Cu_2O powder	hydrothermal	nanoparticle	150	100	50	[12]
Cu_2O	solvothermal synthesis	nanocluster	225	74	50	[13]
Cu_2O	solvothermal synthesis	spherical	87	100	50	[14]
Cu_2O	hydrothermal	nanorod	245	100	50	This work

The specific charge capacities of P-Cu_2O electrode and R-Cu_2O are 415 and 380 $mAh \cdot g^{-1}$, respectively. Although the P-Cu_2O electrode exhibits a slightly higher initial charge and discharge capacity than the R-Cu_2O electrode, the former can maintain a reversible capacity of 62 $mAh \cdot g^{-1}$ with only 20% capacity retention after 50 cycles, while the R-Cu_2O electrode can still maintain the reversible capacity of 245 $mAh \cdot g^{-1}$ with 59% retention rate. Moreover, the R-Cu_2O electrode exhibits a higher initial Coulombic efficiency (71% initially) than the P-Cu_2O electrode. As shown in Table 1, the comparisons of our work versus other previously related studies have been conducted. There are four different morphologies of Cu_2O synthesized by other methods, displaying various cycle performance. In those previous works, Cu_2O film shows the better performance. After 50 cycles, the reversible capacity of 258 $mAh \cdot g^{-1}$ at current density of 37 $mA \cdot g^{-1}$ can be obtained. Compared with our work, although it shows a slightly higher capacity, its charge/discharge current is much lower than ours. Ours is nearly

three time of its. Therefore, our R-Cu$_2$O electrode exhibits more excellent electrochemical cycle performance. According to the previous studies[15-19], this is most likely because the rod-shaped cuprous oxide has shorter ion diffusion channel, smaller volume expansion and better conductivity than the other morphologies.[8]

EIS test was performed to further prove the difference between the R-Cu$_2$O and P-Cu$_2$O electrodes. Figure 3a-b shows EIS data for all cells that completed discharge in the 1st, 5th, 10th, 15th, 20th cycle over a frequency range of 0.01-10^5 Hz, in which the fitting circuit is embedded. As seen in Figure 3a, the charge-transfer resistance of 351, 302, 260, 200 and 125 Ω can be observed in the R-Cu$_2$O, corresponding to the 1st, 5th, 10th, 15th, 20th cycle, respectively. Figure 3b shows the EIS data of the P-Cu$_2$O electrodes, indicating that 425, 310, 264, 213 and 127Ω can be obtained at the 1st, 5th, 10th, 15th, 20th cycle, respectively. Therefore, according to the above analysis, R-Cu$_2$O has lower charge-transfer resistance than P-Cu$_2$O, which is similar to the study of LiMn$_2$O$_4$ [20] nanorod and may be extended to other rod-like materials, providing reference for the design and synthesis of high-performance battery materials. To further compare their performance differences, according to the previous studies[21-25], the quantitative analysis of Na ion diffusion coefficient have been conducted as follow equation.

$$D_{Na^+} = (RT)^2/2A^2n^4F^4C^2\sigma^2 \quad (1)$$

where R is the gas constant, T is the Kevin temperature, A represent the area of the electrode, n is the number of transferred electron, F is the Faraday constant, C is the content of the Na ions and σ is the Warburg factor obtained from the slope of fitted line in Figure 3c-d. As shown in Figure 3e, the Na ion diffusion coefficient of 3.83×10^{-16}, 5.81×10^{-16}, 4.92×10^{-16}, 16.17×10^{-16} and 6.24×10^{-16} have been displayed in P-Cu$_2$O electrodes, at the 1st, 5th, 10th, 15th, 20th cycle, respectively. And the Na ion diffusion coefficient of 2.34×10^{-16}, 3.53×10^{-16}, 11.34×10^{-16}, 17.81×10^{-16} and 6.84×10^{-16} have been observed in R-Cu$_2$O electrodes, at the 1st, 5th, 10th, 15th, 20th cycle, respectively. Therefore, at 1st and 10th cycle, the R-Cu$_2$O electrodes display the lower Na ion diffusion coefficient, reflecting the worse electrochemical performance than P-Cu$_2$O. However, the bigger Na ion diffusion coefficient can be observed after 10th cycle, which indicates the better electrochemical performance obtained in R-Cu$_2$O electrodes after 10 cycles. Thus, the result of Na ion diffusion coefficient is well in line with the cycle performance shown in Figure 2b.
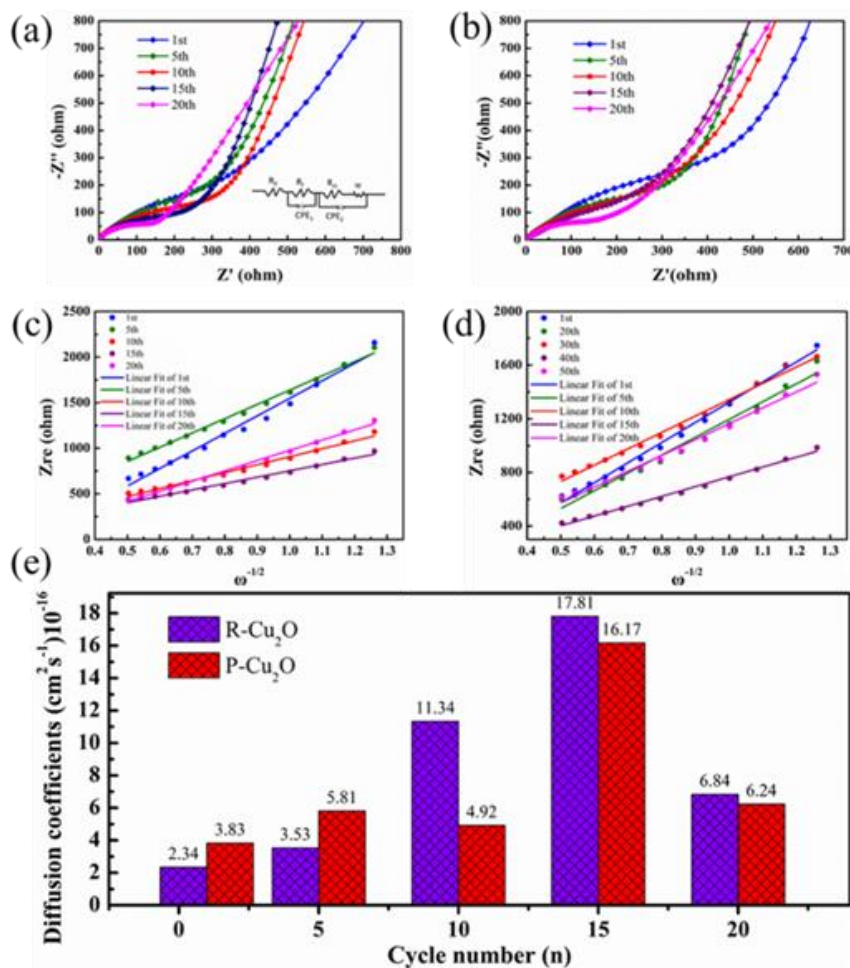
Figure 3. Nyquist plots of (a) R-Cu_2O and (b) P-Cu_2O, (c)-(d) the plot of the relationship of Zre and $\omega^{-1/2}$ in low frequencies. (e) diffusion coefficient of R-Cu_2O and P-Cu_2O.

4. CONCLUSION

High-purity cuprous oxide nanorods and nanoparticles as sodium battery electrode material were successfully synthesized via a hydrothermal method. As validated by SEM, XRD and XPS, the final synthesis product had high purity, good morphology, uniform size, and P space group. The electrochemical tests showed that the specific charge capacity of the cuprous oxide nanorods was 380 mAh·g^{-1}, and a reversible capacity of 245 mAh·g^{-1} with 59% retention rate can be obtained after 50 cycles at a current density of 100 mA·g^{-1}. However, in the cuprous oxide nanoparticles, a capacity of 62 mAh·g^{-1} with 20% capacity retention after 50 cycles can be maintained, indicating the better cycle performance in R-Cu_2O as sodium ion battery materials. In addition, the quantitative analysis of Na ion diffusion coefficient have been conducted, the higher Na ion diffusion coefficient can be observed in R-Cu_2O electrode after 10 cycles, reflecting it has a better electrochemical performance than R-Cu_2O electrode after 10 cycles. In summary, this work might provide a reference for the selection of the shape of energy storage materials.

References

1. K. Sakaushi, E. Hosono, G. Nickerl, T. Gemming, H. Zhou, S. Kaskel, J. Eckert, *Nat. Commun.*, 4 (2013) 1485.
2. Z. Xiaojie, Q. Wei, L. Dongsheng, Y. Dong, H. Bingwen, S. Zhuo, P. Likun, *Chem. Commun.*, 51 (2015) 16413-16416.
3. H. Huang, Y. Liu, J. Wang, M. Gao, X. Peng, Z. Ye, *Nanoscale,* 5 (2013) 1785-1788.
4. L.J. Fu, J. Gao, T. Zhang, Q. Cao, L.C. Yang, Y.P. Wu, R. Holze, H.Q. Wu, *J. Power Sources*, 174 (2007) 1197-1200.
5. G. Prabhakaran, R. Murugan, *Adv. Mater.*, 938 (2014) 114-117.
6. C.H. Kuo, C.H. Chen, M. Huang, thinsp, *Adv. Funct. Mater.,* 17 (2010) 3773-3780.
7. W. Chen, W. Zhang, C. Lin, L. Zeng, M. Wei, *J. Alloys Compd.*, 723 (2017) 172-178.
8. Y.-M. Lin, P. R. Abel, A. Heller, C. Buddie Mullins, *J. Phys. Chem. Lett.*, 2 (2015) 2885-2891.
9. J. Zhou, F. Jiang, S. Li, Z. Xu, W. Sun, X. Ji, Y. Yang, *J. Solid State Electrochem.*, 23 (2019) 1991-2000.
10. Z. Hu, H. Liu, *J. Mater. Sci.*, 26 (2015) 5405-5408.
11. J.Y. Xiang, X.L. Wang, X.H. Xia, L. Zhang, Y. Zhou, S.J. Shi, J.P. Tu, *Electrochim. Acta*, 55 (2010) 4921-4925.
12. Y.T. Xu, Y. Guo, C. Li, X.Y. Zhou, M.C. Tucker, X.Z. Fu, R. Sun, C.P. Wong, *Nano.*, 11 (2015) 38-47.
13. W. Liu, G. Chen, G. He, W. Zhang, *J. Nanopart.*, 13 (2011) 2705.
14. K. Chen, D. Xue, *CrystEngComm.* 15 (2013) 1739-1746.
15. Y.Q. Qiao, X.L. Wang, J.P. Zhou, J. Zhang, C.D. Gu, J.P. Tu, *J. Power Sources*, 198 (2012) 287-293.
16. L. Zhang, B. Wu, L. Ning, D. Mu, C. Zhang, W. Feng, *J. Power Sources*, 240 (2013) 644-652.
17. K. Chen, D. Xue, *Mater. Focus,* 2 (2013) 35-38.
18. Y.M. Jiang, K.X. Wang, X.X. Guo, X. Wei, J.F. Wang, J.S. Chen, *J. Power Sources*, 214 (2012) 298-302.
19. M.K. Devaraju, T. Tomai, I. Honma, *Electrochim. Acta*, 109 (2013) 75-81.
20. K. Hariprasad, N. Naresh, B.N. Rao, M. Venkateswarlu, N. Satyanarayana, *Mater. Today,* 3 (2016) 4040-4045.
21. J. Zhou, S. Li, W. Sun, X. Ji, Y. Yang, *Inorg. Chem. Front.*, 6 (2019) 1217-1227.
22. S. Li, H. Tang, G. Peng, J. Feng, X. Ji, *ACS Appl. Mater. Interfaces,* 10 (2018) 6378-6389.
23. L. Chen, J.-D. Liu, S.-Q. Zhang, *J. Inorg. Mater.*, 28 (2013) 1127-1131.
24. L. He, X.Z. Liao, K. Yang, Y.S. He, W. Wen, Z.F. Ma, *Electrochim. Acta*, 56 (2011) 1213-1218.
25. X. Du, H. Zhao, L. Yao, Z. Zhang, A. Kulka, K. Świerczek, *Electrochim. Acta*, 228 (2017) 100-106.